Study of typical space wave–particle coupling events possibly related with seismic activity*

Zhang Zhen-Xia(张振霞)[a)†], Wang Chen-Yu(王辰宇)[b)], Shen Xu-Hui(申旭辉)[c)], Li Xin-Qiao(李新乔)[d)], and Wu Shu-Gui(吴书贵)[a)]

[a)] *National Earthquake Infrastructure Service, China Earthquake Administration, Beijing* 100045, *China*
[b)] *School of Physics, Peking University, Beijing* 100871, *China*
[c)] *Institute of Earthquake Science, China Earthquake Administration, Beijing* 100045, *China*
[d)] *Institute of High Energy Physics, Chinese Academy of Sciences, Beijing* 100049, *China*

(Received 21 January 2014; revised manuscript received 14 April 2014; published online 10 August 2014)

Based on the DEMETER satellite, we found two space wave–particle coupling events during February 2010 that took place in the range of the McIlwain parameter L (1.27 ∼ 1.37). There are strong spatial and temporal correlation between the particle bursts (PBs) and the electromagnetic disturbances of the coupling events. The two PBs show different energy spectrum characteristics, while the corresponding electromagnetic disturbances concentrated on different frequency ranges. In agreement with the prediction of the theory of wave–particle interaction, we conclude that the two wave–particle interactions can be probably explained as follows: one is electron-dominant precipitation with energy of 0.09 MeV∼0.2 MeV induced by a VLF electromagnetic wave with the frequencies of 14 kHz∼20 kHz, and another is proton-dominant precipitation with energies of 0.65 MeV∼2.85 MeV induced by a VLF electromagnetic wave with the frequency of ≤ 100 Hz. For the first time, these particle bursts' origins, from electrons or protons detected by the Instrument for the Detection of Particles (IDP) on board, are inferred by theoretical calculation, although the instrument has no ability to identify the particle species.

Keywords: particle burst, VLF electric disturbance, wave–particle interaction

PACS: 94.20.wj, 94.30.Tz, 93.85.Rt **DOI:** 10.1088/1674-1056/23/10/109401

1. Introduction

There are many factors that cause high-energy particle acceleration, precipitation and short-term, sharp particle counting rates to increase (particle bursts, or PBs), consisting of ground-based VLF EM transmssions, lightning and thunderstorms, ground nuclear tests and blasts, seismic activity, volcanoes, and so on. The main mechanism is that the EM wave, radiated from those events, couples with the energetic particle in the radiation belt by wave–particle interaction. The interaction accelerates the particle by changing the momentum of the particle, or scatters the pitch angle of the particle and makes them enter the bounce or drift loss cone. So that a mass of energetic particle accumulates at a certain McIlwain parameter L value to induce the particle precipitation, loss or particle burst.

Many effects of electron belts induced by man-made VLF ground-based transmitters obey the theoretical model of wave–particle interaction. Earlier, Inan *et al.* applied a test-particle model of the gyroresonant wave–particle interaction for calculating the precipitation characteristics of the particle flux by a VLF transmitter.[1] They found that the precipitation of the particle is controlled by the pitch angle distribution near the edge of the loss cone. Horne *et al.*[2] studied the mechanism of electron acceleration by waves in the outer radiation belt. They showed that the electrons could be accelerated by electromagnetic waves at frequencies of a few kHz, which can also increase the electron flux by more than three orders of magnitude over the observed timescale of one to two days. Based on the DEMETER (Detection of Electro–Magnetic Emissions Transmitted from Earthquake Regions) satellite, Sauvaud and Maggiolo observed enhancements in the 100 keV–600 keV drift-loss cone electron fluxes at L values between 1.4 ∼ 1.7 induced by NWC transmitter.[3] They calculated the variation of the energy of enhanced electron fluxes with L by the first-order cyclotron resonance theory of wave–particle interaction and obtained consistent results with the observation. Graf *et al.* analyzed the energetic electron flux increase near the loss cone induced by ground-based VLF transmissions of NPM observed via satellite-based detection, and compared the precipitating flux with predictions based on ray-tracing analyses of wave propagation and wave–particle interactions.[4] They indicated that the detection rate is attributed to the orientation of the DEMETER particle detector and obtained the agreement between the observations and theory. Wang *et al.* explained the relationship between the radiation belt electron precipitation observed by DEMETER and the man-made VLF signals in the NPM experiment by the theory of quasi-linear diffusion with resonant interaction, and indicated that most of the non-correlation is caused

*Project supported by the Spark Plan for Earthquake Science and Technology of China Earthquake Administration (Grant No. XH12066), the National Natural Science Foundation of China (Grant No. 11103023), and the Director Foundation of National Earthquake Infrastructure Service (Grant No. NEIS201402).

†Corresponding author. E-mail: zxzhang@neis.gov.cn

© 2014 Chinese Physical Society and IOP Publishing Ltd

by the restriction of the pitch angle measurement of IDP.[5] Li *et al.* analyzed the energy spectrum of the NWC electron belts in detail using the on-off method and explained the pitch angle range observed by the quasi-linear diffusion equation of wave–particle theory.[6] The illustrations of the precipitation of the inner radiation belt electrons, induced by VLF transmitters and their explanation by wave–particle interaction, are also included in the work of Inan *et al.*[7]

In addition to the man-made VLF transmitter, there are many observations on the energetic electron precipitation and particle bursts caused by seismic activity, observed by satellite detectors. The representative works in this subject include the correlation between energetic particle burst and seismic activity based on the MARIA experiment studied in the papers [8–10]. Fidani and Battistion performed a detailed analysis on the short-term and sharp increases in high energy particle counting rates and their correlations to seismic activity based on the whole period of ten years' burst activity from NOAA data.[11]

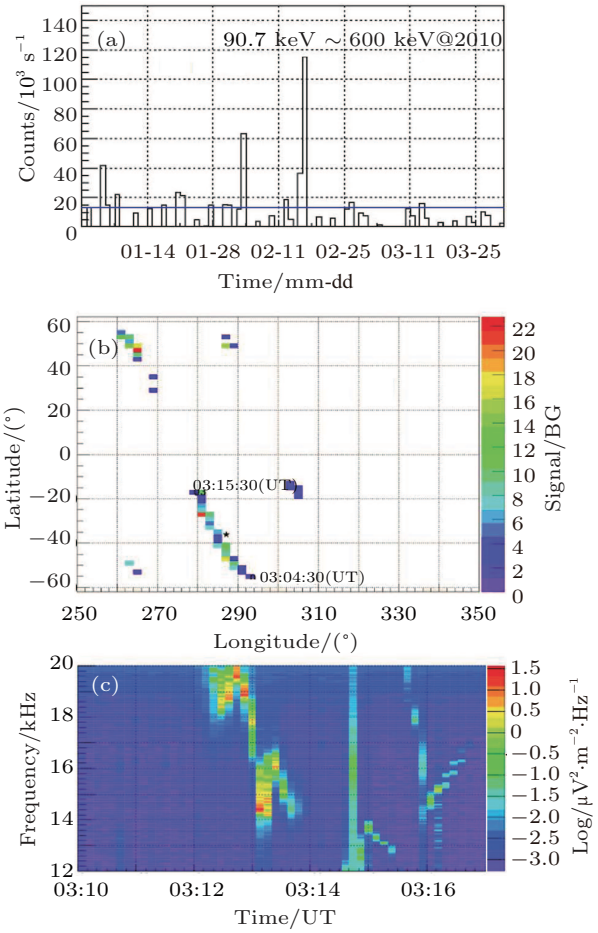


Fig. 1. (color online) All observed figures for PB1 from orbit 30109 on 16th February. (a) The distribution of averaged high-energy charged particle counting rates in 2010. (b) The distribution of position and the duration UT of the energetic particle burst in which the value of signal over average background is equal or larger than 2. The black star denotes the position of the epicenter of the Chile earthquake. (c) The disturbance of the VLF electric spectrum in the ionosphere over the epicenter detected by the DEMETER satellite from the same orbit 30109.[14]

The DEMETER satellite with a 700-km altitude, 98.3°-inclination orbit[12] serves from June 2004 to December 2012. An onboard instrument for particle detection (IDP)[13] measures 72.9 keV∼2.35 MeV electrons with 8.9-keV resolution in burst mode at one sample per second, and the electric field instrument (ICE) measures the electric field fluctuations of 0 kHz∼20 kHz in burst mode. Based on the credible measurement of electric field and energetic particle flux, we can study the particle precipitation and particle burst events and the wave–particle interaction between them and the VLF waves in detail.

When we look for the ionosphere disturbance in the link of the Chile earthquake on 27th February 2010, we find two particle burst events and the corresponding electric field disturbance occurring over the epicenter based on Satellite observation,[14] with the figures shown in Figs. 1 and 2. The energy spectra of the PBs exhibits different distribution structures for the two PBs. In this paper, by calculating the quasi-linear diffusion coefficients for field-aligned electromagnetic waves, we analyze qualitatively the coupling properties of the two PBs and the corresponding VLF electric spectrum disturbance according to the information of their pitch angle, energy spectrum, frequency range, and so on.

2. Observations

The DEMETER satellite, with a quasi-Sun-synchronous orbit, flies downward (from north to south) during local daytime and flies upward (from south to north) during local nighttime. The orbital period is 102.86 minutes. Here we select the satellite data of the upward orbit to perform statistical analysis as the electromagnetic wave can transmit into the ionosphere in night more easily. We analyzed the high-energy particle flux data sample detected by IDP in the first three months of 2010. The charged particle counting rates were considered in three energy regions, 90 keV∼600 keV, 600 keV∼1000 keV, and 1000 keV∼2350 keV, respectively. We selected the satellite orbits which fly over the epicenter region (71°00′ W, 30°00′ S) within the longitude range of 10 degrees and an L value of 0.1. So there are total 42 orbits across the epicenter region of the Chile earthquake during seismic activity in the first three months of 2010. Each orbit can fly across the epicenter region in several minutes.

In Fig. 1, plot (a) displays the distribution of high energy charged particle average counting rates in 2010,[14] from which we can see the peak of the average counting rates very clearly shown on 16th, February in the lower energy region of 90 keV∼600 keV, named PB1, coming from the upward orbit data of 30109. The distribution of the flux enhancement of the PBs with two times flux over the averaged value of background is shown in plot (b). The selected criterion is: signal/BG$\geq$ 2, in

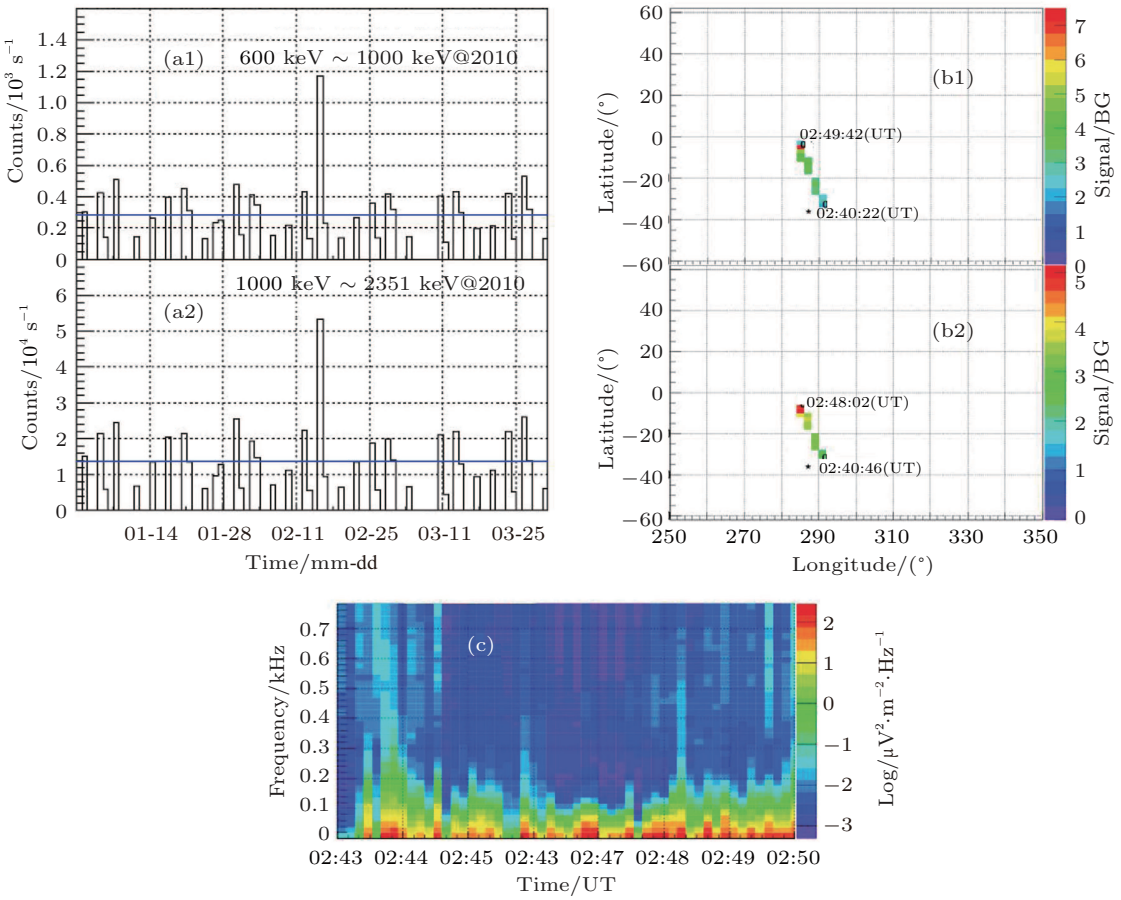


Fig. 2. (color online) All observed figures for PB2 from orbit 30094 on 15th February. Plots of panels (a1) and (a2) denote the distribution of averaged high-energy charged particle counting rates. Plots of panels (b1) and (b2) denote the distribution of position and the duration UT of the energetic particle burst, for 600 keV∼1000 keV and 1000 keV∼2351 keV energy channels respectively, in which the value of signal over average background is equal or larger than 2. The black star denotes the position of the epicenter of the Chile earthquake. (c) The disturbance of the VLF electric spectrum in the ionosphere over the epicenter detected by the DEMETER satellite from the same orbit 30094.[14]

which is denoted the real flux in every pixel and BG denotes the averaged value of flux of all revisited orbits in the first three months of year 2010 over the same focus region. The disturbance of the electric field in the ionosphere over the same region in the same orbit number 30109 detected by the DEMETER satellite is shown in plot (c). In Fig. 2, we present the distribution of high-energy charged particle average counting rates from the orbit number 30094, the position distribution of the flux enhancement, and the corresponding disturbance of the electric field in the ionosphere over the same region with the same orbit number 30094. The peak of the average counting rates appear in the energy channel of 600 keV∼1000 keV and 1000 keV∼2350 keV from the upward orbit data, which is named PB2.

Both PBs for different energy channels exceed about 4 to 6 times the average value of the counting rates. The obvious particle counting rate enhancement also appears in the northern hemisphere mirror point conjugate of the epicenter, induced by the bounce motion of particles between north and south poles along the geomagnetic field line.

Corresponding to the 30109 orbit on 15th February, the frequency range of the electric field disturbance is around 14 kHz to 20 kHz, and corresponding to the 30094 orbit on 16th February, the frequency range of the disturbance is less than 100 Hz.

Table 1 shows the observation time contrast for the PBs and the VLF electric enhancements. From this table, we can easily find there exits strong temporal correlation between the energetic particle bursts and the VLF electric field disturbance, so they are likely to originate from the same VLF EM source, then the wave–particle interaction takes place in the ionosphere at the altitude of DEMETER satellite.

Table 1. The parameter contrast of high-energy particle bursts and the corresponding VLF electric distribution (VLF). Here the pitch angle denotes the equatorial pitch angle of two PBs. PB1 denotes the particle burst from the 30109 orbit, PB2 denotes that from the 30094 orbit.

Event	Energy/frequency	Time/UT	Time/UT	Pitch angle/(°)
PB1	90 keV–200 keV		03:04:30–03:15:30	21.1–29.8
PB2	150 keV–1000 keV	02:40:22–02:49:42		21.4–30.1
PB2	1 MeV–2.35 MeV	02:40:46–02:48:02		21.4–30.1
VLF1	< 100 Hz	02:43:42–02:50:00		
VLF2	14 kHz–20 kHz		03:12:00–03:14:00	

3. Spectrum of PBs

In order to study the energy spectrum characteristics of the PBs described above, we select the data sample in the first three months of 2010 over the epicenter region of the Chile earthquake eliminating the data of 30109 and 30094 orbits, then take it as the background data and compare the energy spectrum of the PBs to the background, shown in Fig. 3.

From the energy spectrum profile, it can be confirmed that the energy of the particle counting rate enhancement from 30109 orbit focus on 0.09 MeV∼0.2 MeV, and that from the 30094 orbit focus on 0.15 MeV∼2.35 MeV. While the corresponding VLF electric spectrum disturbances coming from the same orbits to the PBs have the EM frequency of 14 kHz∼20 kHz and less than 100 Hz, respectively. The details are concluded in the Table 1.

There are very big differences for the frequency of the VLF wave in the wave–particle interaction between the two couplings, one distributes in 14 kHz–20 kHz, another in less than 100 Hz. Under the same conditions of L value, the equatorial pitch angle, the longitude and latitude, and so on, there must be a certain mechanism driving the coupling process, for instance, the two PBs may originate from different particle species: electron and proton. IDP has no ability to identity the particle species, so we have to verify this assumption by theoretical calculation.

Since the detected electron efficiency is very low in an energy range larger than 1 MeV, we assume that the particles of PB2 are likely to come from the protons. This supposition is proved to be correct in the theoretical calculation analysis in the next section. The data of level-1 was reconstructed in the condition of thinking all the particles as electrons, so we need to recalculate the incident energy spectrum for the PB2 particles by taking them as protons. In IDP the optic has an aluminum foil with a thickness of 6 μm to stop protons with energies lower than 500 keV.[13] The detected energy spectrum can be derived by counting for the electron efficiency profile. The detected energy spectrum is the same as the incident energy spectrum of proton, since the efficiency of a proton penetrating through the aluminum foil is almost 100%. So the corrected incident energy range for the particles in PB2 is derived to be 0.65 MeV∼2.85 MeV, shown in Fig. 3(d).

IDP has no angular identification ability to the incident particles, but fortunately they can record the pitch angle by calculating the direction between the axis of the IDP aperture and the local magnetic field. The pitch angles for the PBs observed here are presented in Fig. 4. The particle pitch angles are distributed within $76^\circ \sim 78^\circ$ and $80^\circ \sim 82^\circ$ for the two PBs respectively (see Table 1 for details). At the latitude of $32.8^\circ \sim 39.8^\circ$ corresponding to the selected region above the Chile earthquake, the equatorial pitch angles are derived to be: $21.1^\circ \sim 29.8^\circ$ and $21.4^\circ \sim 30.1^\circ$.

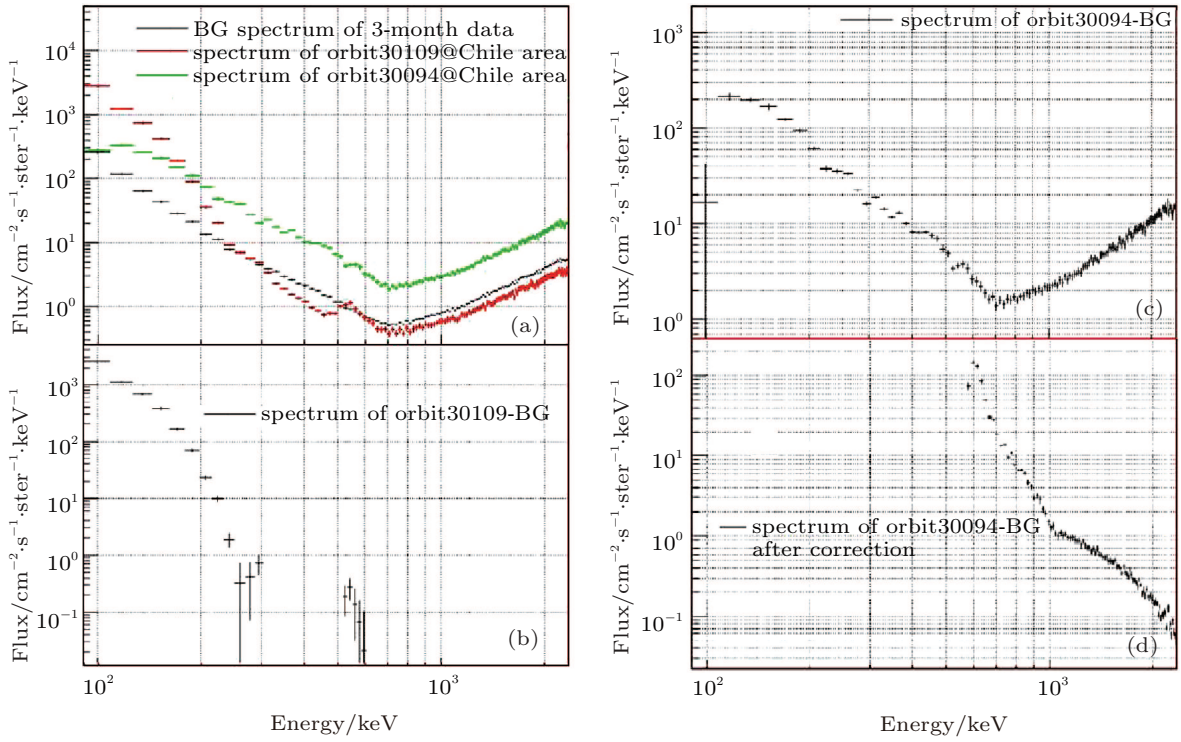


Fig. 3. (color online) Energy spectrum of PBs and their background. (a) The black profile graph with error bar denotes the average energy spectrum for the first three months of 2010 except those of the 15th and 16th February, and the red one of the 16th February (30109 orbit), the green one for the 15th February (30094 orbit). (b) Energy spectrum of PB1 from 30109 subtracting that of background. (c) Energy spectrum of PB2 from 30094 subtracting that of background. (d) Energy spectrum of PB2 from 30094 subtracting that of background, after performing the corrections of efficiency and incident-deposition energy relation of proton.

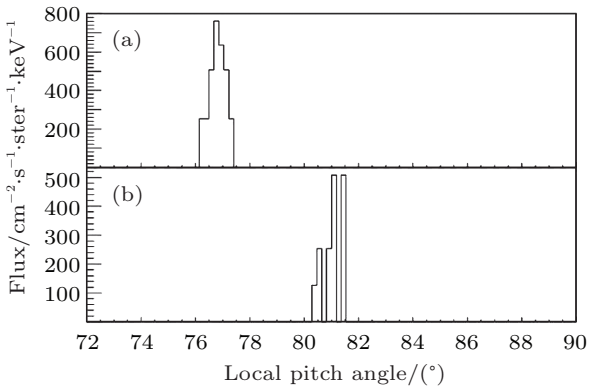


Fig. 4. The local pitch angle distribution of the PBs: (a) for PB1 from 30109 orbit, (b) for PB2 from 30094 orbit.

4. Verification of pitch angle diffusion equation in wave–particle interaction theory

Despite that magnetospheric physics has been studied for more than 40 years, the dynamics of the Earth's particle radiation belts are not well understood and have been attracting people's research interests. Among many papers for discussing the processes which govern the transportation, acceleration, and loss of radiation belt electrons, what engages people's attention is the results of Refs. [15] and [16], which assesses the influence of wave–particle interactions on radiation belt electron dynamics. In the early work[17] on pitch angle scattering of radiation belt particles, the gyroresonant wave–particle interaction was thought to play a crucial role in magnetoshperic physics. The work of Summers[18] developed a special form of the quasi-linear diffusion coefficients corresponding to (R-mode or L-mode) electromagnetic waves with a Gaussian spectral density propagating in a hydrogen plasma. They derived a collisionless Vlasov equation for the particle distribution function to the second order in perturbation and obtained the diffusion equation. In the inner radiation belts, the particle velocities generally are much larger than the typical phase velocities of waves, so pitch angle diffusion plays a dominant role in the wave–particle interaction.

Originating from the Fokker–Planck equation,[19] the quasi-linear diffusion equation with only pitch-angle diffusion coefficients for cyclotron resonant interaction with field-aligned electromagnetic waves of arbitrary spectral density can be written as

$$\frac{\partial f}{\partial t} = \frac{1}{\sin\alpha}\frac{\partial}{\partial\alpha}\left(D_{\alpha\alpha}\sin\alpha\frac{\partial f}{\partial\alpha}\right), \tag{1}$$

where, for one particle of certain species σ, charge q, and rest mass m_σ, $f(\alpha,E,L)$ is the density function in the gyrophase-averaged phase space, which depends on the equatorial pitch angle α, the kinetic energy E, and the McIlwain parameter L.

Assuming that the wave frequency spectrum density obeys a Gaussian distribution, the local pitch angle diffusion coefficient of wave–particle interaction is deduced as follows:

$$D_{\alpha\alpha} = \frac{\pi}{2}\frac{1}{\nu}\frac{\Omega_\sigma^2}{|\Omega_e|}\frac{1}{(E+1)^2}\sum_s\sum_j\frac{R(1-x\cos\alpha/y\beta)^2|F(x,y)|}{\delta x|\beta\cos\alpha - F(x,y)|} \cdot\exp\left[-\left(\frac{x-x_m}{\delta x}\right)^2\right], \tag{2}$$

where E is the dimensionless particle kinetic energy given by $E = E_k/(m_\sigma c^2) = \gamma - 1$; $\beta = \nu/c = [E(E+2)]^{1/2}/(E+1)$; B is the Earth's magnetic field and $R = |\delta B_s|^2/B_0^2$ is the ratio of the energy density of the turbulent magnetic field to that of the background field. $x_m = \omega_m/|\Omega_e|$, $\delta x = \delta\omega/|\Omega_e|$, $s = 1$ for R-mode wave and $s = -1$ for L-mode wave. $j = 1,2,\ldots,N$ is the root number of satisfying the resonance condition,

$$\omega_j - \nu\cos\alpha k_j = -s\frac{q}{|q|}\frac{|\Omega_\sigma|}{\gamma}, \tag{3}$$

$F(x,y) = \mathrm{d}x/\mathrm{d}y$ ($x = \omega/|\Omega_e|$, $y = ck_i/|\Omega_e|$) is determined from the dispersion equation of electron or proton as follows:

$$\left(\frac{ck}{\omega}\right)^2 = 1 - \frac{(1+\epsilon)/\alpha^*}{(\omega/|\Omega_e| - s)(\omega/|\Omega_e| + s\epsilon)}, \tag{4}$$

where

$$\alpha^* = \Omega_e^2/\omega_{pe}^2 \tag{5}$$

is an important cold-plasma parameter; ϵ is the rest mass ratio of electron and proton; $|\Omega_e| = e|B_0|/(m_e c)$ denotes the electron gyrofrequency and $\omega_{pe} = (4\pi N_0 e^2/m_e)^{1/2}$ is the plasma frequency, where N_0 denotes the particle number density in ionosphere at the altitude of satellite observation.

From the VLF electric spectrum distribution and energy spectrum of PBs, the typical wave–particle interaction takes place in the ionosphere. Furthermore, the coupling energy of the particle and the frequency of VLF wave take on a specific correlation, as listed in Table 1.

Assuming that the wave–particle interaction occurs only within the equatorial plane, we can calculate the equatorial pitch angle diffusion coefficient for the electron coupling with an R-mode electromagnetic wave and the proton coupling with an L-mode electromagnetic wave. The parameters are chosen as follows: the wave amplitude $\delta b = 10$ pT, the equatorial magnetic field determined by a dipole model $B = 3.11\times10^{-5}/L^3$ T. The equatorial plasma density N is equal to $N_0\times(2/L)^4$ cm^{-3} according to the study.[20,21] Due to the location of PBs in the South Atlantic Anomaly where the average particle counting ratio is much larger than other regions in the ionosphere, we select particle density $N_0 = 1.8\times10^4$ cm^{-3} which is at least reasonable in magnitude compared to the satellite detection result. The other parameters used in the theory calculation can be found in every plot.

Eventually, we obtained the nice agreement between the DEMETER observation and the quasi-linear diffusion equation calculation, as long as the PBs of 30109 is explained to originate dominantly from the electron and the PBs of 30094 from a proton, that is, the electron couples with an R-mode EM

wave and the proton with an L-mode EM wave in the wave–particle interaction mechanism. Figure 5 shows the profile of the equatorial pitch angle diffusion coefficient $D_{\alpha\alpha}$ depending on the pitch angle distribution.

In Fig. 5, for the coupling of an electron and an R-mode EM wave, we choose the bandwidth of a wave spectrum with $\mathrm{d}f = 100$ Hz, and for that of a proton and an L-mode EM wave, the frequency bandwidth is $\mathrm{d}f = 1$ Hz. The L value with $L = 1.32$ in the center of the observation region is selected. The range between two dashed lines in the figure indicates the observation limit of the DEMETER satellite. We can find the pitch angle of a wave–particle interaction with the electron energy 0.1 MeV and VLF EM wave frequency from 15 kHz∼19 kHz distributes in around $20^\circ \sim 30^\circ$ and just enters the sight of IDP. As for the proton versus L-mode EM wave, considering the parameter range of PBs and the VLF EM wave observed, we select several cases with different interaction parameters and calculate the pitch angle diffusion coefficient. The protons with energy 0.65 MeV interact with a VLF wave with frequencies of 15 Hz, 18 Hz, 20 Hz; the protons with energy 2.85 MeV interact with waves of 7 Hz, 9 Hz, 11 Hz. Their pitch angle diffusion can completely or partially fall into the observed range of equatorial pitch angle around $20^\circ \sim 30^\circ$ between the two dashed lines in the plots.

Under the condition of a given equatorial pitch angle α, EM frequency f and other parameters, the particle energy of the quasi-linear diffusion coefficient theory relies on the L value. The reports showed a decrease in energy with increasing L from cyclotron resonance.[22,23] In Fig. 6, we present the coupled energy of the electron and proton depending on L value by theoretical calculation, panels (a) and (b) for electron coupling with R-mode EM wave, panels (c) and (d) for proton coupling with L-mode EM wave. The equatorial pitch angles in panels (a) and (c) used in the theoretical calculation are selected to be: 20° and 30° in panels (b) and (d), which is just consistent with the range of observed PBs listed in Table 1. We find that, within the range of L values $1.27 \sim 1.37$, the energy of particles calculated corresponding to the shadow region in each plot is almost consistent with the energy of the PBs observed by DEMETER, that is, 0.1 MeV∼0.2 MeV for an electron and 0 MeV∼3.4 MeV for a proton.

The relations between the particle energy and the VLF EM wave in the wave–particle interaction are shown in Fig. 7 derived by the resonance condition (3) and the dispersion equation (4).

For an electron coupling with an R-mode EM wave, the particles with energies of 0.09 MeV–0.15 MeV interact with the VLF EM wave with frequencies of 12 kHz∼20 kHz. For a proton versus an L-mode wave, particles with energies of 0.65 MeV∼2.85 MeV interact with the VLF wave with a frequency of less than 100 Hz. These calculation results agree well with the observation range of PBs and VLF electric disturbance, see the detail in Table 1.

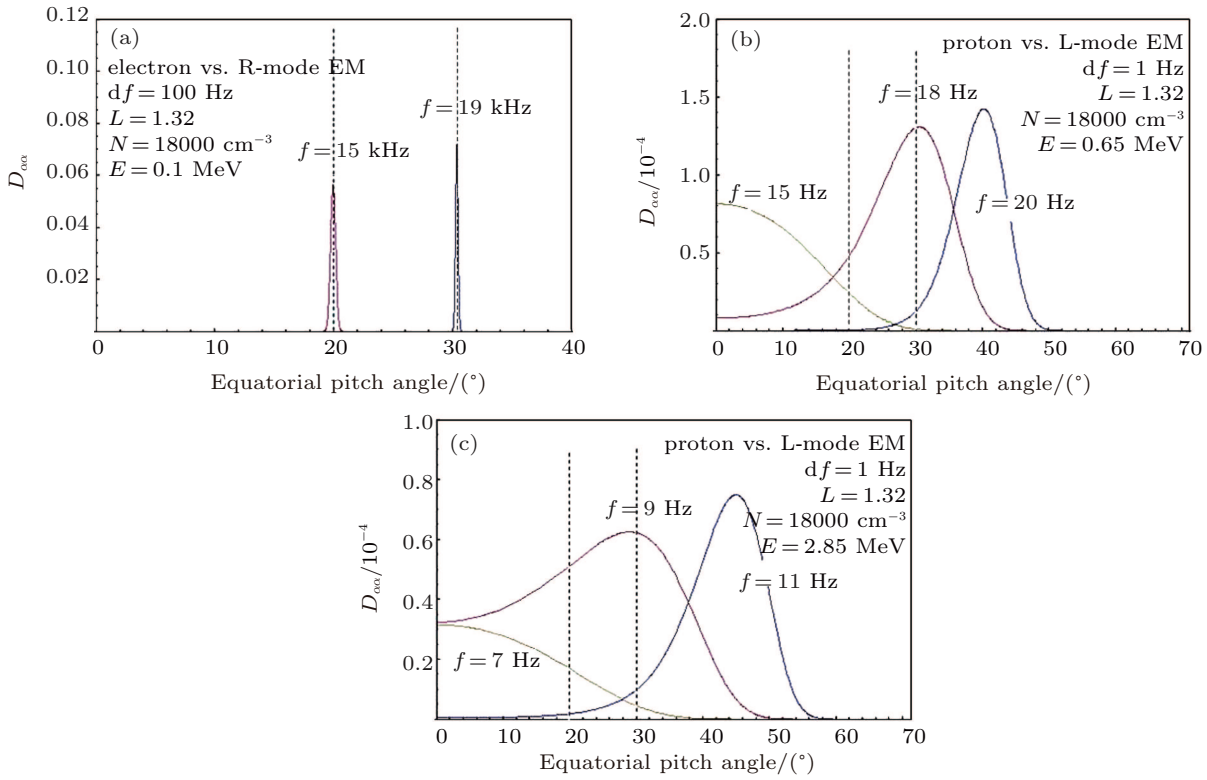


Fig. 5. (color online) The dependence of pitch angle diffusion coefficient distribution on equatorial pitch angle. The parameters used here are: L value 1.32 and particle density 1.8×10^4 cm^{-3}. (a) For the electron coupling with R-mode EM wave with the frequency bandwidth 100 Hz. (b) For the 0.65-MeV proton coupling with L-mode EM wave. (c) For the 2.85-MeV proton coupling with L-mode EM wave. The vertical dashed lines denote the satellite observation range in pitch angle.

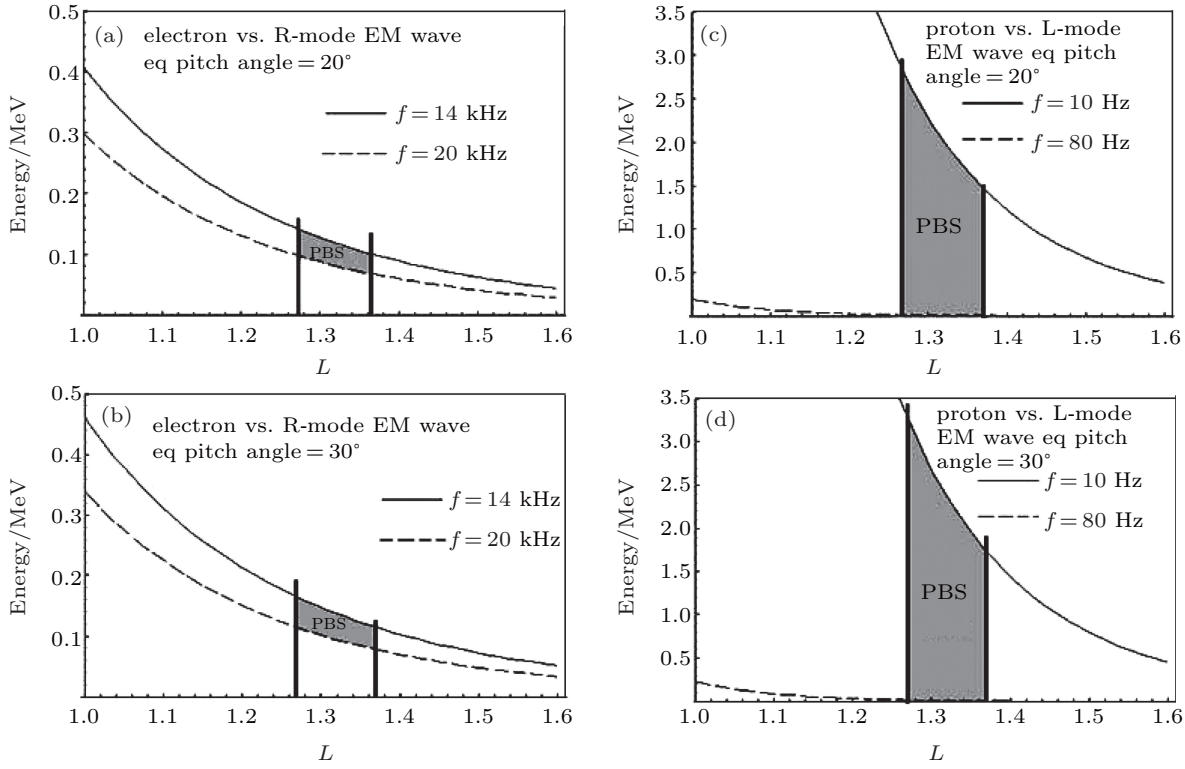


Fig. 6. The particle energy calculated by quasi-linear diffusion coefficient equation, shown in the shadow region. Parameter L ranges from 1.27 to 1.37, just in accordance with the range of PBs observed. The solid and dashed curves represent the different wave frequencies used in the calculation.

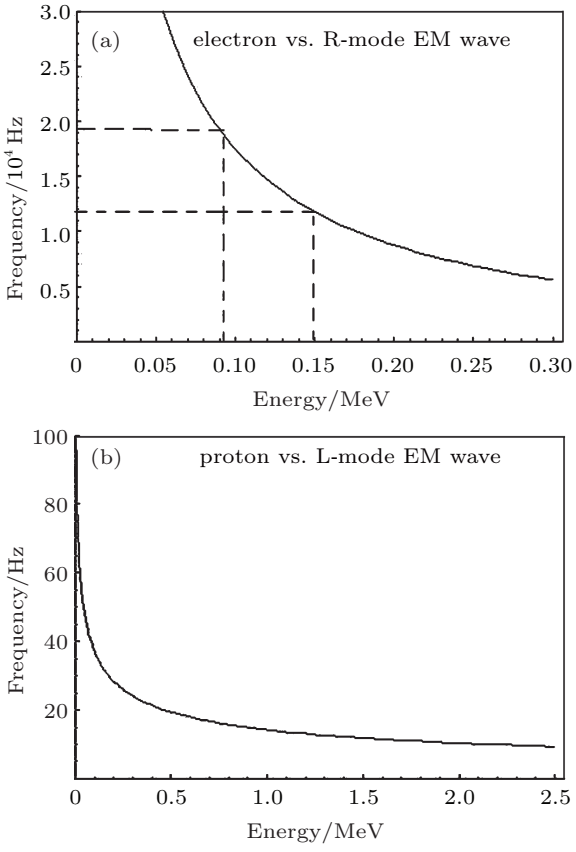


Fig. 7. The coupling relation of the frequency of EM wave and the energy of particles calculated by the theory of quasi-linear diffusion coefficients, (a) for the electron coupling with an R-mode EM wave, (b) for the proton coupling with an L-mode EM wave.

5. Discussion and summary

For the study of the high-energy particle counting rate enhancement and VLF electric disturbance observed simultaneously in the ionosphere, we have analyzed the energy spectrum of PBs and showed the pitch angle distribution of them and pointed out that the typical wave–particle interaction takes place, which induces the energetic charged particle entering the drift loss cone, causing particle counting rate enhancement locally in the ionosphere. The energy range for the two PBs distributes around 0.09 MeV∼0.2 MeV and 0.65 MeV∼2.85 MeV, but the frequency of a VLF wave coupling with particles has much more different values, 14 kHz∼20 kHz and less than 100 Hz.

If we regard the particles in PBs as electrons and protons respectively, the agreement with observation is obtained by calculation of the pitch angle quasi-linear diffusion coefficient equation. We verify the supposition by checking three kinds of correlation formula: pitch angle diffusion coefficient $D_{\alpha\alpha}$ depending on pitch angle α, the coupled particle energy depending on the McIlwain parameter L, and the relation between coupled particle energy and VLF wave frequency. So it confirms that the PBs and VLF electric spectrum disturbance are caused by the same VLF EM wave source, and proves that we find one typical wave–particle interaction based on the DEMETER satellite.

For the first time, with the inability to identify particle species of IDP on board DEMETER, by wave–particle inter-

action calculation, we point out the particle bursts' origin accurately as either from an electron or proton dominant source. In addition, with the PBS and electric spectrum disturbance appearing simultaneously over the Chile earthquake epicenter about 10 days before the earthquake, if there is really certain link between the PBs and VLF electric disturbance and seismic activity as argued by the authors in Ref. [14], then this is also the first time that we have obtained evidence of precursor information of seismic activity, that is, the electron and proton counting rate enhancement in the ionosphere was simultaneously observed by satellite.

The consistent results with observation also proved the correctness and rationality of the theory of the quasi-linear diffusion coefficient equation, in application to the particle precipitation and wave–particle interaction analysis in the low orbital satellite observation in the ionosphere. It is worthwhile saying that the errors, associated with the negligence of higher-order resonances, are smaller than the inaccuracies associated with uncertainties in the input values for the plasma density and latitudinal distribution of the waves. Although reasonable assumptions have been made, there is still some limitation and a long road to describe precisely the observation for the theory. Such as, the accuracy of the plasma density playing an important role in theory always depends on the more accurate measurement of satellite detection to ionosphere. Many researchers studied the outer radiation dynamics of two-dimensional (2D) momentum-pitch-angle diffusion equation of energetic electrons interacting with a whistler wave, and the translation process of a whistler wave during little strong geomagnetic activities,[24–26] and there are still other related works[27,28] focusing on the properties of wave propagation and wave–particle interaction. So we will continue further study based on those works and attempt to perform some quantitative calculations.

Laboratory measurements have indicated that rock samples under stress can radiate EM energy in a wideband spectrum, and that light can be observed.[29] Estimations of the size of the earthquake preparation zone are thought to range from 150 km for magnitude 5 EQs to more than 2.5×10^3 km for magnitude 8.[30] So if it is true that the seismic activity radiates EM waves and the waves can propagate into the ionosphere and diffuse the energetic particles by wave–particle interaction, then we can monitor the particle change to investigate the seismic activity. So we need to explore the theoretical model to provide support for this hypothesis.

In this paper, we have only performed qualitative analysis for the EM waves coupling with energetic particles in the ionosphere. In order to systematically and quantitatively research seismic electromagnetic radiation in lithosphere–atmosphere–ionosphere and the subsequent ionospheric disturbance, in the future we will still apply the proper propagation model of the EM wave, such as the ray tracing method, to calculate the power reduction of waves and the wave normal angles and fields of whistler mode waves in the ionosphere.[31,32] In the process, we will use parameters closer to real conditions, including a more realistic geomagnetic field model rather than the dipole magnetic field, non-uniform magnetic flux density, and more realistic plasma layer density. In terms of wave–particle interaction, we will consider the effect of the radial diffusion of a particle and apply the nonlinear cyclotron resonant interaction of energetic electrons and coherent VLF waves, to quantitatively calculate the precipitation or space distribution change of energetic particles.[33]

Although the position we selected the data to study is located in the South Atlantic Anomaly (SAA), the saturation of the IDP detector does not take place. In a previous paper,[14] we showed the distribution of high-energy charged particle counting rates in the epicenter region for three different energy regions, from left to right plots are the distributions for the year 2007, 2008, and 2009. From these figures, we can find the maximum value of averaged counting rates in the first plot of 90.7 keV∼600 keV @2007 is close to 300×10^3, while the maximum value of the particle burst is only less than 120×10^3. So there is no saturation of the IDP detector above SAA.

The energy spectra in Ref. [14], with the flux increase above 700 keV, did not indicate a pile-up effect of the electronics. The shape of the spectra with an increase above 700 keV is due to the efficiency correction.[13] In addition, this case of energy spectrum shape is also the same when the flux is very low. The data we downloaded from the DEMETER website are the science data of level-1 after performing the efficiency correction. So basically, there is no pile-up for the data we used. The data we used in this work are reliable.

References

[1] Inan U S, Chang H C and Helliwell R A 1985 *J. Geophys. Res.* **90** 359

[2] Horne R B, Thome R M, Shprits Y Y, Meredith N P, Glauert S A, Smith A J, Kanekal S G, Baker D N, Engebretson M J, Posch J L, Spasojevic M, Inan U S, Pickett J S and Decreau M E 2005 *Nature* **437** 227

[3] Sauvaud J A, Maggiolo R, Jacquey C, Parrot M, Berthelier J J, Gamble R J and Rodger C J 2008 *Geophys. Res. Lett.* **35** L09101

[4] Graf K L, Inan U S, Pddyachiy D, Kulkarni P, Parrot M and Sauvaud J A 2009 *J. Geophys. Res.* **114** A07205

[5] Wang P, Wang H Y, Ma Y Q, Li X Q, Lu H, Meng X C, Zhang J L, Wang H, Shi F, Xu Y B, Yu X X, Zhao X Y and Wu F 2011 *Acta Phys. Sin.* **60** 039401 (in Chinese)

[6] Li X Q, Ma Y Q, Wang P, Wang H Y, Lu H, Zhang X M, Huang J P, Shi F, Yu X X, Xu Y B, Meng X C, Wang H, Zhao X Y and Parrot M 2012 *J. Geophys. Res.* **117** A04201

[7] Inan U S, Golkowski M, Casey M K, Moore R C, Peter W, Kulkarni P, Kossey P, Kennedy E, Meth S and Smit P 2007 *Geophys. R. L.* **34** L02106

[8] Voronov S A, Galper A M, Kirillov-Ugryumov V G, Koldashov S V, Mikhallov V V, Popov A V and Chesnokov V Y 1987 *Proc. 20th ICRC* **4** 451

[9] Voronov S A, Galper A M, Koldashov S V, *et al.* 1989 *Cosmic Res.* **27** 629

[10] Parrot M 2009 *Anomalous Seismic Phenomena: View from Space in Electromagnetic Phenomena Associated with Earthquakes* (Trivandrum: Transworld Research Network) pp. 629–631

[11] Fidani C and Battistion R 2008 *Nat. Hazards Earth Syst. Sci.* **8** 1277-1291
[12] Parrot M, Benoist D, Berthelier J J, Blecki J, Chapuis Y, Colin F, Elie F, Fergeau P, Lagoutte D, Lefeuvre F, Legendre C, Lévêque M, Pincon J L, Poirier B, Seran H C and Zamora P 2006 *Nat. Planet. Space Sci.* **54** 441
[13] Sauvaud J A, Moreau T, Maggiolo R, Treilhou J P, Jacquey C, Cros A, Coutelier J, Rouzaud J, Penou E and Gangloff M 2006 *Nat. Planet. Space Sci.* **54** 502
[14] Zhang Z X, Li X Q, Wu S G, Ma Y Q, Shen X H, Chen H R, Wang P, You X Z and Yuan Y H 2012 *Chin. J. Geophys.* **55** 1581 (in Chinese)
[15] Gendrin R 2001 *The Role of Wave Particle Interactions in Radiation Belts Modeling, in Sun–Earth Connection and Space Weather* (Bologna: SIF) p. 151
[16] Horne R B 2002 *The Contribution of Wave-Particle Interactions to Electron Loss and Acceleration in the Earth's Radiation Belts During Geomagnetic Storms, in Review of Radio Science* (Hoboken, NJ: John Wiley) **33** pp. 801–828
[17] Kernel C F and Petschek H E 1966 *J. Geophys. Res.* **71** 1
[18] Summers D 2005 *J. Geophys. Res.* **110** A08213
[19] Melrose D B 1980 *Nonthermal Processes in Diffuse Magnetized Plasmas* (New York: Gordon and Breach) Vol. 2
[20] Angerami J J and Thomas J O 1964 *J. Geophys. Res.* **69** 4537
[21] Inan U S, Chang H C and Helliwell R A 1984 *J. Geophys. Res.* **89** 2891
[22] Koons H C, Edgar B C and Vampola A L 1981 *J. Geophys. Res.* **86** 640
[23] Chang H C and Inan U S 1983 *J. Geophys. Res.* **88** 318
[24] Zheng H N, Su Z P and Xiong M 2008 *Chin. Phys. Lett.* **25** 3515
[25] Xiao F L, He Z G, Zhang S, Su Z P and Chen L X 2011 *Chin. Phys. Lett.* **28** 039401
[26] Su Z P, Zheng H N and Xiong M 2009 *Chin. Phys. Lett.* **26** 039401
[27] Jiang H, Yang X X and Lin M M 2011 *Chin. Phys. B* **20** 019401
[28] Zhang Z X, Wang C Y, Li Q and Wu S G 2014 *Acta. Phys. Sin.* **63** 079401 (in Chinese)
[29] Cress G O, Brady B T and Rowell G A 1987 *Geophys. Res. Lett.* **14** 331
[30] Dobrovolsky I P, Zubkov S I and Miachkin V I 1979 *Pageoph.* **117** 1025
[31] Starks M J, Quinn R A, Ginet G P, Albert J M, Sales G S, Reinisch B W and Song P 2009 *J. Geophys. Res.* **113** A09320
[32] Tao X, Bortnik J and Friedrich M 2010 *J. Geophys. Res.* **115** A07303
[33] Inan U S, Bell T F and Helliwell R A 1978 *J. Geophys. Res.* **83** 3235